Radial modal dependence of the azimuthal spectrum after parametric down-conversion

Yingwen Zhang,[1] Filippus S. Roux,[1,*] Melanie McLaren,[1,2] and Andrew Forbes[1,2,3]
[1]*CSIR National Laser Centre, PO Box 395, Pretoria 0001, South Africa*
[2]*Laser Research Institute, University of Stellenbosch, Stellenbosch 7602, South Africa*
[3]*School of Chemistry and Physics, University of KwaZulu-Natal, Private Bag X54001, 4000 Durban, South Africa*
(Received 26 February 2014; published 14 April 2014)

The radial degrees of freedom of the biphoton states that are produced in spontaneous parametric down-conversion (SPDC) in the Laguerre-Gaussian (LG) basis are investigated, theoretically and experimentally. We calculated the theoretical azimuthal Schmidt numbers for different combinations of radial indices and found that a larger azimuthal Schmidt number is obtained for higher radial indices of the signal and idler beams. Moreover, larger azimuthal Schmidt numbers are also obtained when the difference between the two radial indices increases. Comparing these theoretical predictions with the azimuthal Schmidt numbers obtained from experimentally measurements, we found good agreement. Experimentally we demonstrated that it is possible to obtain a threefold increase in the azimuthal Schmidt number while maintaining a reasonable coincidence count rate by using LG modes with slightly larger radial indices.

DOI: 10.1103/PhysRevA.89.043820 PACS number(s): 42.65.Lm, 42.50.Tx, 42.50.Dv, 03.67.Bg

I. INTRODUCTION

Entanglement is a distinct phenomenon of quantum mechanics. A proper understanding and use of entanglement can lead to significant technological advances in communication, computing, and cryptography [1]. In recent years there has been much interest in the entanglement among optical modes that carry orbital angular momentum (OAM) [2]. These modes are capable of carrying large amounts of information due to the infinite-dimensional nature of OAM and thus are of significant interest for quantum information [3]. Entanglement in the OAM has also been used to demonstrate the violation of Bell's inequality [2,4,5].

Pairs of photons entangled in OAM can be readily produced through spontaneous parametric down-conversion (SPDC) [6–8]. The degree of entanglement of a quantum state can be quantified by the Schmidt number [9,10]. When restricted to the OAM degrees of freedom (by fixing the radial degrees of freedom) the equivalent quantity is called the azimuthal Schmidt number, which is also an indication of the width of the OAM spectrum, i.e., the spiral bandwidth [10–14]. Hence, a large spiral bandwidth indicates that an OAM entangled quantum state contains more OAM degrees of freedom that can be used to encode quantum information.

The Laguerre-Gaussian (LG) modes are OAM eigenstates and are a popular basis for photonic quantum information application. They also carry a radial index p, which governs their radial dependence. It has been shown [10,15] that both azimuthal and radial degrees of freedom are required to saturate the full Schmidt number of a quantum state produced by SPDC. A number of techniques have been investigated to increase the spiral bandwidth of LG modes, including increasing the pump beam size and manipulating the SPDC phase matching conditions [13,16–18]. Nevertheless, the radial degrees of freedom are often neglected, summed over or fix to their simplest case $p = 0$ as it is challenging to generate accurate LG modes with a nonzero radial index as mentioned in [19]. It has been shown that the azimuthal Schmidt number depends on the radial dependence of the chosen basis state and that the azimuthal Schmidt number obtained from Bessel-Gaussian (BG) modes, which are also OAM eigenstates, are larger than for LG modes with $p = 0$ [20,21].

In this paper we investigate, theoretically and experimentally, how the azimuthal Schmidt number depends on the chosen radial dependence for an LG basis. For this purpose the radial indices are fixed to arbitrary values in the signal and idler beams, respectively. We restrict the analysis here to the case of degenerate collinear type I SPDC with a Gaussian pump.

II. THEORY

A. Coincidence amplitude

The coincidence counts in a SPDC experiment are proportional to the modulus square of the down-converted probability amplitude $|\mathcal{M}|^2 = |\langle\Psi_f|\mathcal{P}|\Psi_{\rm in}\rangle|^2$, where $\mathcal{P}$ represents the SPDC process and $\Psi_{\rm in}$ and Ψ_f are the initial and final photon states, respectively. For type I phase matching, with collinear signal and idler beams and degenerate signal and idler frequencies ($\omega_{\rm s} = \omega_{\rm i} = \frac{1}{2}\omega_{\rm p}$), the probability amplitude in the paraxial limit is

$$\mathcal{M} = \Omega_0 \int M_{\rm s}^*(\mathbf{q}_1) M_{\rm i}^*(\mathbf{q}_2) \times M_{\rm p}(\mathbf{q}_1+\mathbf{q}_2) S(\mathbf{q}_1-\mathbf{q}_2) \frac{d^2q_1}{(2\pi)^2}\frac{d^2q_2}{(2\pi)^2}, \quad (1)$$

where Ω_0 is an overall constant that determines the conversion efficiency, $\mathbf{q} = q_x\hat{x} + q_y\hat{y}$ is the two-dimensional transverse part of the three-dimensional wave-vector $\mathbf{k}$, the angular spectra of the mode profiles of the signal, idler, and pump beams are given by $M_{\rm s}(\mathbf{q})$, $M_{\rm i}(\mathbf{q})$, and $M_{\rm p}(\mathbf{q})$, respectively, and $S(\mathbf{q}_1 - \mathbf{q}_2)$ is the phase matching function.

The pump beam is a Gaussian beam, so that

$$M_{\rm p}(\mathbf{q}) = \sqrt{2\pi}\, w_p \exp\left(-\frac{w_p^2}{4}|\mathbf{q}|^2\right), \quad (2)$$

where w_p is the radius of the pump beam waist.

*fsroux@csir.co.za

The signal and idler beam profiles are LG modes. Here we represent the angular spectra of these LG modes by

$$M_{\mathrm{s,i}}^{\ell,p}(\mathbf{q}) = \mathcal{N}\frac{1}{p!}\left[\partial_\eta^p \partial_\mu^{|\ell|}\mathcal{G}\right]_{\eta,\mu=0}, \tag{3}$$

where $\mathcal{G}$ is the generating function for the LG modes [22], μ and η are generating parameters for the azimuthal and radial indices, respectively, and

$$\mathcal{N} = \left[\frac{2\pi 2^{|\ell|}p!}{(p+|\ell|)!}\right]^{1/2}. \tag{4}$$

The generating function is given by

$$\mathcal{G} = \frac{1}{1+\eta}\exp\left[\frac{i(q_x \pm i q_y)w\mu}{2(1+\eta)} - \frac{\left(q_x^2+q_y^2\right)w^2(1-\eta)}{4(1+\eta)}\right], \tag{5}$$

where w is the radius of the beam waists and the sign in the exponent is given by the sign of ℓ. For simplicity we assume that the radii of the beam waists of the signal and idler beams are equal $w_\mathrm{s} = w_\mathrm{i} = w$.

The phase matching function is given by

$$S(\mathbf{q}_1 - \mathbf{q}_2) = \mathrm{sinc}\left(\frac{\beta w_p^2}{8}|\mathbf{q}_1 - \mathbf{q}_2|^2\right), \tag{6}$$

where we define $\mathrm{sinc}(a) = \sin(a)/a$ and β is a dimensionless combination of parameters. The latter is given by

$$\beta = \frac{n_o L \lambda_p}{\pi w_p^2} = \frac{n_o L}{z_R}, \tag{7}$$

where n_o is the ordinary refractive index of the nonlinear crystal, λ_p is the wavelength of the pump, L is the crystal length, and z_R is the Rayleigh range of the pump beam.

The expression in Eq. (1) is a more general version of the integral considered previously [13]. Instead of setting the radial index to zero ($p = 0$) for both the signal and idler beams, we allow their radial indices to have arbitrary values. Using the generating function for LG modes, we are able to solve the more general integral analytically.

Evaluating the integral in Eq. (1) with Eqs. (2)–(7), one finds that, unless the azimuthal indices of the signal and idler modes have equal magnitudes and opposite signs (OAM is conserved), the result is zero. One can therefore set $\ell_\mathrm{s} = -\ell_\mathrm{i} = \ell$. So we express the result of the integration as a generating function for the probability amplitudes $\mathcal{M}$, in terms of explicit azimuthal indices, but with the radial indices of the signal and idler beams implicit in terms of their generating parameters η_s and η_i, respectively. This generating function is given by

$$\mathcal{G}_\ell = \frac{i\alpha^{|\ell|+1}}{\mathcal{B}^{|\ell|+1}\beta}[Z^{|\ell|+1}\Phi(-Z,1,|\ell|+1) - (Z^*)^{|\ell|+1}\Phi(-Z^*,1,|\ell|+1)], \tag{8}$$

where $\Phi(z,m,n)$ is the Lerch transcendent function [23],

$$Z = \frac{(2-i\beta)\mathcal{B}}{\alpha\mathcal{A} + i\beta\mathcal{B}}, \tag{9}$$

$$\mathcal{A} = (1-\eta_\mathrm{s})(1-\eta_\mathrm{i})\alpha + 2(1-\eta_\mathrm{s}\eta_\mathrm{i}), \tag{10}$$

$$\mathcal{B} = 2(1+\eta_\mathrm{s})(1+\eta_\mathrm{i}) + (1-\eta_\mathrm{s}\eta_\mathrm{i})\alpha, \tag{11}$$

$$\alpha = \frac{w^2}{w_p^2}, \tag{12}$$

and β is defined in Eq. (7). Note that the generating parameters for the radial indices of the signal and idler beams are only found inside $\mathcal{A}$ and $\mathcal{B}$. To obtain the probability amplitude for particular radial indices p and q of the signal and idler beams, respectively, one performs the following operation

$$\mathcal{M} = \frac{\Omega_0}{w_p}\mathcal{N}_{pq}\left[\partial_{\eta_\mathrm{s}}^p \partial_{\eta_\mathrm{i}}^q \mathcal{G}_\ell\right]_{\eta_\mathrm{s},\eta_\mathrm{i}=0}, \tag{13}$$

where

$$\mathcal{N}_{pq} = \left[\frac{2(|\ell|!)^2}{\pi(p+|\ell|)!(q+|\ell|)!p!q!}\right]^{1/2}. \tag{14}$$

For the $p = 0$ case, one sets $\eta_\mathrm{s} = \eta_\mathrm{i} = 0$. As a result $\mathcal{A} = \mathcal{B} = 2 + \alpha$ and the expressions simplify to those obtained by Miatto *et al.* [14].

B. Thin crystal limit

All the experimental parameters are contained in the dimensionless parameters α [Eq. (7)] and β [Eq. (7)]. The latter is the ratio of the nonlinear crystal length L to the Rayleigh range of the pump beam z_R, times the ordinary refractive index, which is of order 1. In most experiments $L \ll z_R$. As a result $\beta \ll 1$. In this limit, the probability amplitude $\mathcal{M}$ can be expressed as

$$\mathcal{M} = \frac{\Omega_0}{w_p}\mathcal{N}_{pq}\left(\frac{2}{\mathcal{A}}\right)^{|\ell|+1} + O(\beta^2). \tag{15}$$

In the case where $\beta = 0$, the argument of the phase matching function in Eq. (6) becomes zero, with the result that the phase matching function is equal to 1. As a result, one can Fourier transform Eq. (1) to the coordinate domain. The result is a three-way overlap integral, given by

$$\mathcal{M} = \Omega_0 \int m_\mathrm{p}(\mathbf{x}) m_\mathrm{s}^*(\mathbf{x}) m_\mathrm{i}^*(\mathbf{x})\, d^2x, \tag{16}$$

where $m_{\mathrm{p,s,i}}(\mathbf{x})$ represents the mode profile of the pump, signal, or idler beam.

C. Schmidt number

To quantify the bandwidth of the spectrum of OAM modes we use the azimuthal Schmidt number, which is defined by

$$\kappa = \frac{1}{\sum_\ell P_\ell^2}, \tag{17}$$

where P_ℓ represents the probability to observe a particular pair of OAM modes for a given set of p indices. It is proportional to the modulus square of the probability amplitude. The coincidence counts $\mathcal{C}_\ell$ obtained in the experiment are proportional to the probabilities P_ℓ. Hence, the azimuthal Schmidt number can be computed by

$$\kappa = \frac{\left(\sum_\ell \mathcal{C}_\ell\right)^2}{\sum_\ell \mathcal{C}_\ell^2}. \tag{18}$$

III. EXPERIMENT

A. Experimental setup

The experimental setup is shown by the diagram in Fig. 1. A 350 mW pump laser beam with a wavelength of 355 nm traversed a 3-mm-thick BBO crystal to produce degenerate,

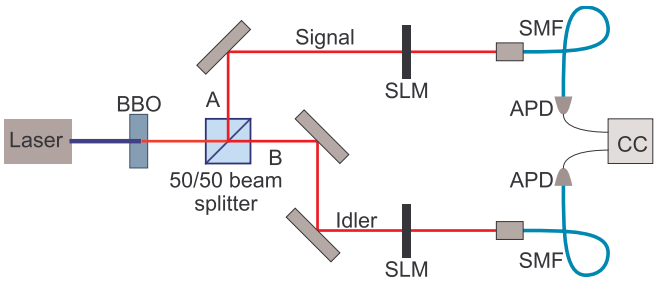

FIG. 1. (Color online) Diagram of the experimental setup used to prepare and measure the OAM entangled photon pairs.

collinear photon pairs with type I phase matching, which are entangled in their OAM degrees of freedom. The beam size of the pump mode profile on the plane of the BBO was 1 mm. The signal and idler beams were separated using a 50:50 beam splitter. Each beam was directed onto a spatial light modulator (SLM) that was used to modulate the beam by the conjugate of the mode which was to be detected. Type-3 complex amplitude modulation given in [24] was used to generate the hologram on the SLMs, the LG mode size used on the hologram was 0.575 mm. The modulated beams were coupled into single mode fibres (SMFs), which extract the Gaussian profile from the beams. The beam size of the Gaussian mode of the SMF, imaged back onto the BBO crystal, was 0.575 mm. Avalanche photodiodes (APDs) that were connected to the other ends of these SMFs, register the photon pairs via a coincidence counter (CC).

B. Modeling the experiment

Due to the experimental parameters of the setup, $\beta = 0.0023$, which means that one can work in the thin crystal limit and use Eq. (16) to model the experiment. The SLMs are usually used to implement the functions of $m_s(\mathbf{x})$ and $m_i(\mathbf{x})$, using complex amplitude modulation [24]. However, the coupling of the beams into the SMFs imply that the integrand must also contain the Gaussian modes of these SMFs. One can therefore express the actual overlap integral that is implemented by the experiment as

$$\mathcal{M} = \Omega_0 \int m_p(\mathbf{x}) m_s^*(\mathbf{x}) m_i^*(\mathbf{x}) G^2(\mathbf{x}) d^2x, \tag{19}$$

where

$$G(\mathbf{x}) = \left(\frac{2}{\pi}\right)^{1/2} \frac{1}{w_0} \exp\left(-\frac{x^2+y^2}{w_0^2}\right) \tag{20}$$

is the mode of the SMF, with radius w_0 when imaged onto the nonlinear crystal. Since the pump is also a Gaussian function, the effect of these extra Gaussian functions is to modify the effective mode size of the pump

$$\exp\left(-\frac{x^2+y^2}{w_p^2}\right) \to \exp\left(-\frac{x^2+y^2}{(w_p')^2}\right), \tag{21}$$

where

$$\frac{1}{(w_p')^2} = \frac{1}{w_p^2} + \frac{2}{w_0^2}. \tag{22}$$

The effective mode size of the pump is smaller than the mode size of the original pump beam. To take the effect of the SMF Gaussian profiles into account in the theory, one merely needs to replace $w_p \to w_p'$ in the expressions in Sec. II. It was found that if one does not take the effect of these SMF Gaussian profiles into account, the theoretical results differ significantly from the experimental results as can be seen in Fig. 2, which shows the azimuthal Schmidt number κ calculated theoretically before and after the SMF Gaussian modes have been taken into account.

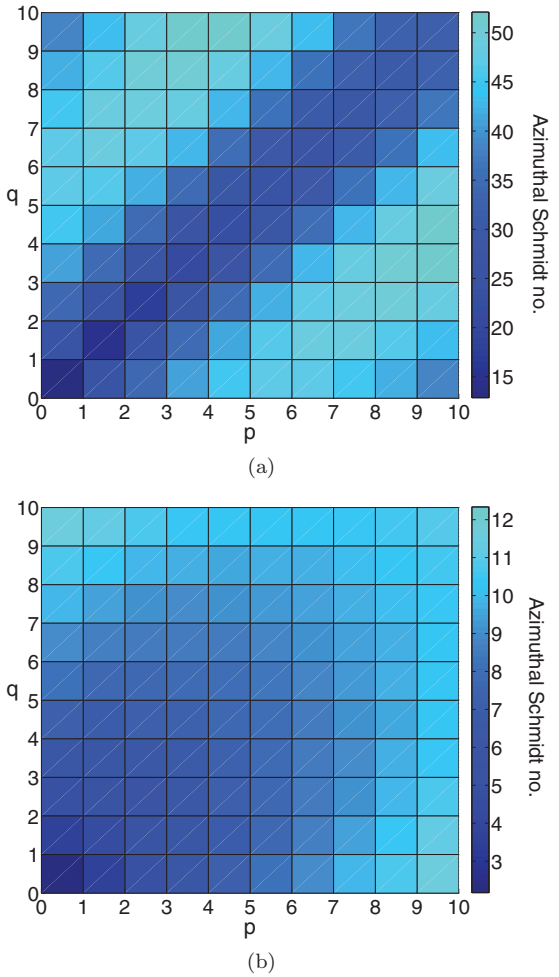

FIG. 2. (Color online) The azimuthal Schmidt numbers κ, calculated in the thin crystal limit using Eq. (16), for p and q running from 0 to 10, showing the difference between (a) the azimuthal Schmidt numbers calculated without taking the SMF modes into account and (b) the azimuthal Schmidt numbers calculated with the SMF Gaussian modes. The parameters used for these calculations are the same as the experimental parameters namely $w_p = 1$ mm, $w = 0.575$ mm, and $w_0 = 0.575$ mm giving $\alpha = 0.331$ for (a) and $\alpha = 2.34$ for (b).

One could in principle modify the modes on the SLMs to compensate for the extra Gaussian profiles coming from the SMFs. However, in practice this can only work if the radial functions of the modes on the SLMs are scale invariant, as in the case of the LG modes with $p = 0$.

C. Results and discussion

Using the setup in Fig. 1, we measured the azimuthal Schmidt number κ for all combinations of p and q running from 0 to 5. The results are shown in Fig. 3. A two-dimensional

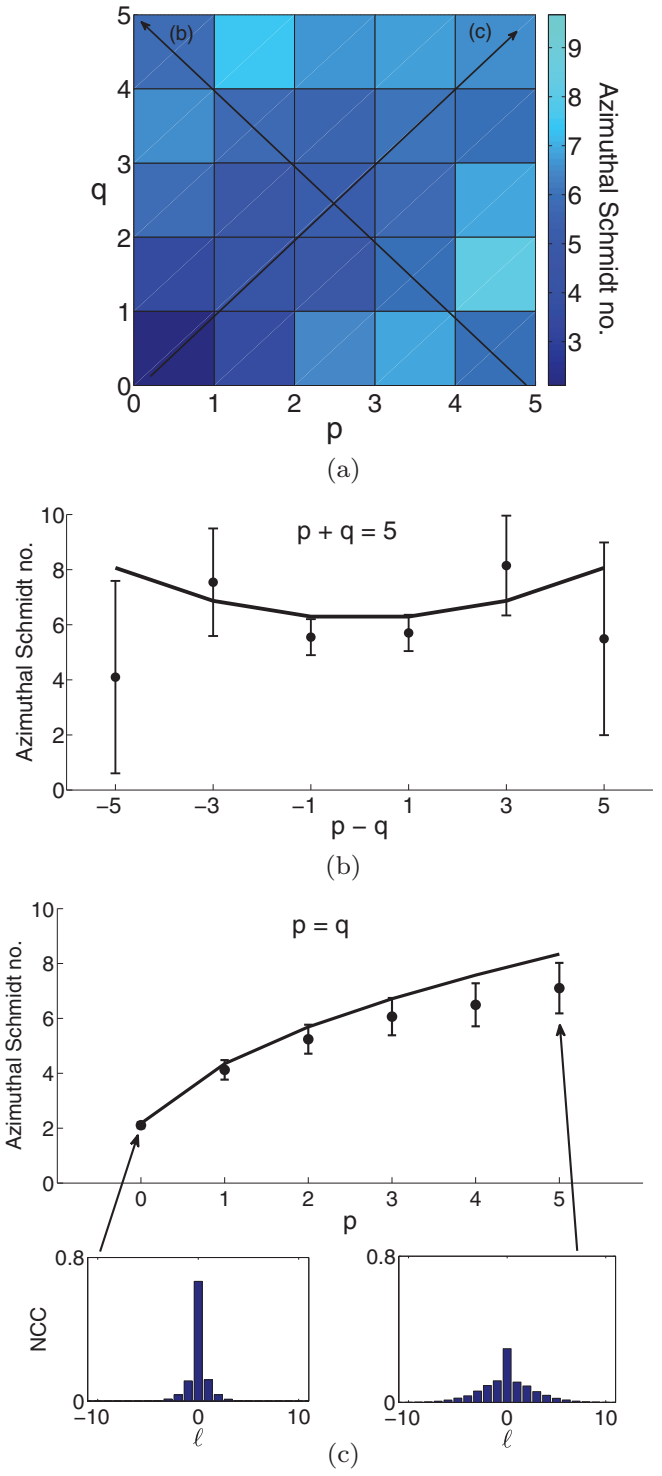

FIG. 3. (Color online) The two-dimensional plot in (a) shows the azimuthal Schmidt number κ as calculated from experimentally measured OAM spectra for radial indices p and q running from 0 to 5. The curves in (b) and (c) show the experimental results (dots) compared to the theoretical results (line) along the diagonals indicated by the arrows in (a). We also show the measured OAM spectra, in terms of normalized coincidence counts (NCC), at $p = q = 0$ and $p = q = 5$ in (c). Error bars represent one standard deviation of the coincidence counts, assuming a Poisson distribution.

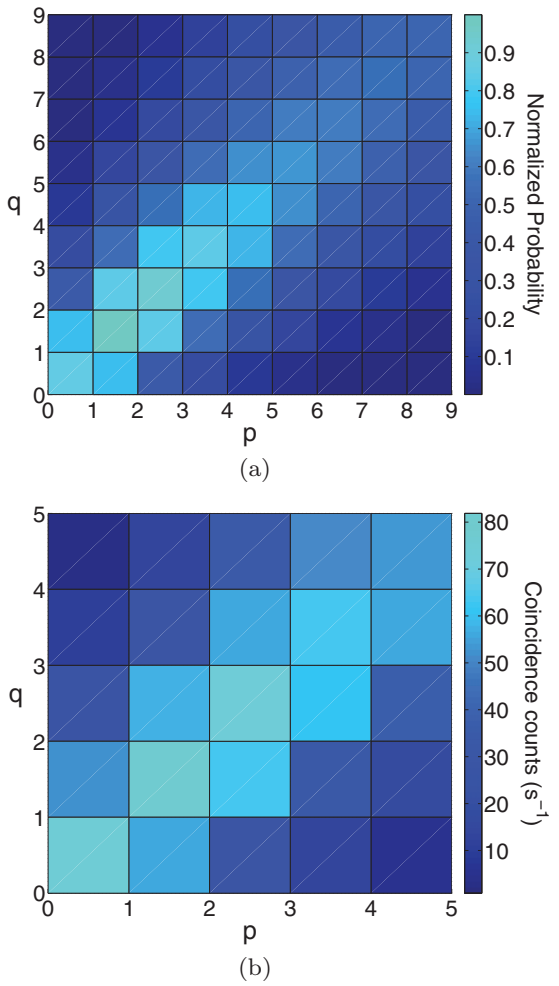

FIG. 4. (Color online) (a) Normalized probabilities P_ℓ determined theoretically for p and q running from 0 to 9 with $\ell = 2$. (b) Coincidence count rate $\mathcal{C}_\ell$ measured experimentally for p and q running from 0 to 5 with $\ell = 2$.

plot of the values of κ is given in Fig. 3(a). The experimental results on the diagonals of Fig. 3(a) are shown in quantitative detail in Figs. 3(b) and 3(c). In Fig. 3(b) we show how the value of κ increases when the difference between the two radial indices $|p - q|$ grows larger and in Fig. 3(c) we show how the value of κ increases for larger radial index $p = q$. We also show the OAM spectra, in terms of normalized coincidence counts ($=C_\ell / \sum C_\ell$), for the two end points in Fig. 3(c).

In general, the experimental results agree with the theory. However, in Fig. 3(b) the errors in the data grow very large at large $|p - q|$ and in Fig. 3(c) the experimental values of κ increase at a slower rate as a function of p than the theoretical values of κ. The larger errors that are obtained for certain combinations of p and q is a result of smaller coincidence counts. To demonstrate this, we show the theoretical detection probabilities and experimental coincidence count rates in Fig. 4. Figure 4(a) shows the theoretical probabilities $P_{\ell,p,q}$ at $\ell = 2$ for p and q running from 0 to 9. The experimentally measured coincidence count rates $\mathcal{C}_{\ell,p,q}$ are shown in Fig. 4(b). As expected, there is a good agreement between the theoretical

probabilities and experimental coincidence count rates. One can see in Fig. 4 that $P_{\ell,p,q}$ and $\mathcal{C}_{\ell,p,q}$ are small when the difference $|p-q|$ is large. In fact, when $|p-q|=5$ [at the two corners of Fig. 4(b)] the coincidence count rates never exceeded 3 counts/s (with background subtracted) for any of the ℓ's. Moreover, $P_{\ell,p,q}$ and $\mathcal{C}_{\ell,p,q}$ decrease toward larger radial index along the $p=q$ diagonal. The smaller values of $\mathcal{C}_{\ell,p,q}$ (or $P_{\ell,p,q}$) give larger error bars, as found in Figs. 3(b) and 3(c).

Apart from the increase in the size of the error bars, we also see a larger disagreement between theory and measured results at the end points of the curve in Fig. 3(c). This disagreement is believed to be caused by a reduced fidelity of the modal function on the SLM when using intensity masking to represent the mode. Due to the limited resolution of the SLM, modal functions with larger p and ℓ indices are rendered with less accuracy, compared to those with smaller p and ℓ indices.

From the above results, we see that, with our experimental parameters, the combination of radial indices that gives the optimal spiral bandwidth, while maintaining good beam quality and acceptable coincidence count rates, are for p and q equal to 1 and 3 (or 3 and 1). The resulting value of the azimuthal Schmidt number κ is approximately 3 times that at $p=q=0$.

IV. CONCLUSION

The effect of the radial index of the LG basis on the spiral (OAM) bandwidth of down-converted photon states is investigated. It is shown both theoretically and experimentally that the spiral bandwidth increases with increasing radial index. Moreover, when the radial index of the signal and idler beams are different the spiral bandwidth increases even further. In other words, although the diagonal modes (those with the same radial indices for the signal and idler beams) are dominant, the off-diagonal modes give larger spiral bandwidths. The experimental setup in this case employs type I SPDC with collinear, degenerate signal and idler beams, and a Gaussian pump. We use the azimuthal Schmidt number to quantify the spiral bandwidth.

For the purpose of the theoretical analysis we obtained analytic expressions for the probability amplitude to detect photon pairs with arbitrary LG modes. Using generating functions for the LG modes, we were able to obtain expressions that apply for any combination of azimuthal and radial indices. For the case when the radial indices are set to zero, our expressions agree with those found in previous work [8,13,14].

Using these expressions we calculated the azimuthal Schmidt number for different combinations of signal and idler beam radial indices and compared them with the experimentally measured azimuthal Schmidt numbers. The agreement between theory and experiment is fairly good provided the radial indices are not too large ($p \lesssim 5$) and the difference between the signal and idler radial index is small ($|p-q| \lesssim 3$). We also demonstrated that it is possible to obtain up to a threefold increase in the azimuthal Schmidt number without a significant loss in coincidence count rate.

When modeling the experimental setup, we found that it is important to take the effect of the Gaussian modes of the SMFs into account in the overlap integral. The contribution from the SMF modes is often overlooked. We showed that the theoretical results can differ significantly when the modes of the SMFs are not included in the overlap integral.

[1] M. A. Nielsen and I. L. Chuang, *Quantum Computation and Quantum Information* (Cambridge University Press, New York, 2010).

[2] B. Jack, A. M. Yao, J. Leach, J. Romero, S. Franke-Arnold, D. G. Ireland, S. M. Barnett, and M. J. Padgett, Phys. Rev. A **81**, 043844 (2010).

[3] G. Molina-Terriza, J. P. Torres, and L. Torner, Nat. Phys. **3**, 305 (2008).

[4] J. Leach, B. Jack, J. Romero, A. Jha, A. M. Yao, S. Franke-Arnold, D. G. Ireland, R. W. Boyd, S. M. Barnett, and M. J. Padgett, Science **329**, 662 (2010).

[5] A. Aiello, S. S. R. Oemrawsingh, E. R. Eliel, and J. P. Woerdman, Phys. Rev. A **72**, 052114 (2005).

[6] A. Mair, A. Vaziri, G. Weihs, and A. Zeilinger, Nature (London) **412**, 313 (2001).

[7] S. Franke-Arnold, S. M. Barnett, M. J. Padgett, and L. Allen, Phys. Rev. A **65**, 033823 (2002).

[8] J. P. Torres, A. Alexandrescu, and L. Torner, Phys. Rev. A **68**, 050301 (2003).

[9] A. Ekert and P. Knight, Am. J. Phys. **63**, 415 (1995).

[10] C. K. Law and J. H. Eberly, Phys. Rev. Lett. **92**, 127903 (2004).

[11] G. Molina-Terriza, J. P. Torres, and L. Torner, Phys. Rev. Lett. **88**, 013601 (2001).

[12] B.-J. Pors, C. H. Monken, E. R. Eliel, and J. P. Woerdman, Opt. Express **19**, 6671 (2011).

[13] F. M. Miatto, A. M. Yao, and S. M. Barnett, Phys. Rev. A **83**, 033816 (2011).

[14] F. M. Miatto, D. Giovannini, J. Romero, S. Franke-Arnold, S. M. Barnett, and M. J. Padgett, Eur. Phys. J. D **66**, 1 (2012).

[15] V. D. Salakhutdinov, E. R. Eliel, and W. Löffler, Phys. Rev. Lett. **108**, 173604 (2012).

[16] M. P. van Exter, A. Aiello, S. S. R. Oemrawsingh, G. Nienhuis, and J. P. Woerdman, Phys. Rev. A **74**, 012309 (2006).

[17] H. Di Lorenzo Pires, H. C. B. Florijn, and M. P. van Exter, Phys. Rev. Lett. **104**, 020505 (2010).

[18] J. Romero, D. Giovannini, S. Franke-Arnold, S. M. Barnett, and M. J. Padgett, Phys. Rev. A **86**, 012334 (2012).

[19] E. Karimi, D. Giovannini, E. Bolduc, N. Bent, F. M. Miatto, M. J. Padgett, and R. W. Boyd, Phys. Rev. A **89**, 013829 (2014).

[20] M. McLaren, M. Agnew, J. Leach, F. S. Roux, M. J. Padgett, R. W. Boyd, and A. Forbes, Opt. Express **20**, 23589 (2012).

[21] M. McLaren, J. Romero, M. J. Padgett, F. S. Roux, and A. Forbes, Phys. Rev. A **88**, 033818 (2013).

[22] F. S. Roux, Phys. Rev. A **83**, 053822 (2011).

[23] A. Jeffrey and D. Zwillinger, *Table of Integrals, Series, and Products* (Elsevier Science, Amsterdam, 2007).

[24] V. Arrizón, U. Ruiz, R. Carrada, and L. A. González, J. Opt. Soc. Am. A **24**, 3500 (2007).